



# Magnesium diffusion in plagioclase: Dependence on composition, and implications for thermal resetting of the $^{26}\text{Al}$ – $^{26}\text{Mg}$ early solar system chronometer



James A. Van Orman<sup>a,\*</sup>, Daniele J. Cherniak<sup>b</sup>, Noriko T. Kita<sup>c</sup>

<sup>a</sup> Department of Earth, Environmental and Planetary Sciences, Case Western Reserve University, 10900 Euclid Avenue, Cleveland, OH 44106, USA

<sup>b</sup> Department of Earth and Environmental Sciences, Rensselaer Polytechnic Institute, Troy, NY 12180, USA

<sup>c</sup> Department of Geoscience, University of Wisconsin–Madison, Madison, WI 53706, USA

## ARTICLE INFO

### Article history:

Received 20 June 2013

Received in revised form 16 October 2013

Accepted 18 October 2013

Available online xxxx

Editor: T.M. Harrison

### Keywords:

cosmochronology  
chondrites  
magma residence time

## ABSTRACT

Experimental data are reported on Mg diffusion in plagioclase crystals with a range of anorthite content ( $x_{\text{An}}$ ), at temperatures between 800 and 1150 °C. Oriented and polished single crystals of anorthite ( $x_{\text{An}} = 0.93$ ), labradorite ( $x_{\text{An}} = 0.67$ ), andesine ( $x_{\text{An}} = 0.43$ ) and oligoclase ( $x_{\text{An}} = 0.23$ ) were each embedded in powered source material enriched in natural MgO or  $^{25}\text{MgO}$  and suspended in a furnace at constant temperature. Diffusion profiles in quenched samples were measured from the polished surface using SIMS depth profiling. The diffusion coefficient does not depend significantly on the Mg concentration gradient, and little anisotropy is observed between the *b* and *c* directions in labradorite. Diffusion coefficients increase systematically with decreasing  $x_{\text{An}}$ , and the entire data set is described by  $\ln D = (-6.06 \pm 1.10) - (7.96 \pm 0.42)x_{\text{An}} - \frac{287 \pm 10 \text{ kJ/mol}}{RT}$ , where *R* is the gas constant, *T* is absolute temperature, and the diffusion coefficient *D* is in  $\text{m}^2/\text{s}$ .  $^{26}\text{Al}$ – $^{26}\text{Mg}$  ages in albite-rich plagioclase are much more easily reset than in anorthite, with closure temperatures up to 120–150 K lower.

© 2013 Elsevier B.V. All rights reserved.

## 1. Introduction

The  $^{26}\text{Al}$ – $^{26}\text{Mg}$  radioactive decay system is one of the most important sources of information on the timing of events in the early solar system. In situ decay of  $^{26}\text{Al}$  (half-life of 0.705 Ma) produces a detectable excess of  $^{26}\text{Mg}$  in phases with high Al/Mg ratios, and its presence provides unequivocal evidence for the formation of the object within several million years of the synthesis of  $^{26}\text{Al}$ . Excess radiogenic  $^{26}\text{Mg}$  has been found in refractory inclusions (CAIs) in chondritic meteorites (e.g., MacPherson et al., 1995; Kita et al., 2013, and references therein), in chondrules (Kita and Ushikubo, 2012, and references therein) and even in metamorphosed ordinary chondrites and achondrites (e.g., Srinivasan et al., 1999; Zinner and Göpel, 2002), and hence may provide a fine-scale chronometer not only for condensation and heating events within the solar nebula but for the assembly and thermal history of planetesimals.  $^{26}\text{Al}$ – $^{26}\text{Mg}$  chronometry depends, however, on the ability to determine the significance of the age implied by excess  $^{26}\text{Mg}$ . Does it correspond to the time of formation of the object, or has it been partially or fully reset by later processing? Perhaps the most important, and best understood, mechanism for resetting of  $^{26}\text{Al}$ – $^{26}\text{Mg}$  ages is by thermally activated diffusive loss of  $^{26}\text{Mg}$

from high Al/Mg phases. Because plagioclase is the most common high Al/Mg phase in meteorites, and the one in which excess  $^{26}\text{Mg}$  is usually best resolved (Lee et al., 1977; Kurahashi et al., 2008; Goodrich et al., 2010; Kita et al., 2012), diffusion data for Mg in plagioclase are critical to determine the susceptibility of  $^{26}\text{Al}$ – $^{26}\text{Mg}$  ages to modification by thermal events. LaTourrette and Wasserburg (1998) determined Mg self-diffusion coefficients in nearly pure anorthite (An<sub>95</sub>; i.e. 95 mol% anorthite) single crystals at 1200–1400 °C. The results of this study provide strong constraints on the resetting of  $^{26}\text{Al}$ – $^{26}\text{Mg}$  ages at high temperatures, in CAIs and other materials that contain anorthitic plagioclase. However, a long extrapolation is required to extend these data to thermal resetting at the much lower temperatures characteristic of metamorphism within planetesimals. Furthermore, application of these data to the more albite-rich plagioclase that is found in high-FeO (Type II; Kunihiro et al., 2004; Kurahashi et al., 2008) chondrules, equilibrated chondrites, and other meteoritic materials such as ureilites (Goodrich et al., 2010), is highly uncertain because no experimental data have yet been published on the dependence of Mg diffusion on plagioclase composition. Studies of other cations in plagioclase indicate a significant dependence of diffusivities on An content, with diffusion faster in more albite-rich plagioclase (Behrens et al., 1990; LaTourrette and Wasserburg, 1998; Cherniak and Watson, 1992, 1994; Giletti and Casserly, 1994; Cherniak, 1995, 2002, 2003).

\* Corresponding author.

E-mail address: james.vanorman@case.edu (J.A. Van Orman).

Magnesium diffusion in plagioclase also provides the basis for time constraints on magmatic processes (Costa et al., 2003, 2008; Drittt et al., 2012). Plagioclase phenocrysts commonly preserve chemical zoning in both trace and major elements that can only be preserved if the crystals' residence at high temperature was short enough to prevent diffusive homogenization. The compositional zoning profiles can be modeled to provide quantitative constraints on the time these phenocrysts experienced in the magma chamber between development of the original zoning profile and eruption. Magnesium profiles in plagioclase are particularly well suited to this purpose because Mg often can be analyzed with sufficient precision by electron microprobe and because its diffusivity is relatively rapid, providing access to information on the annual to millennial timescale. The influence of plagioclase composition on Mg diffusion is particularly important for these applications, because the zoning of trace elements such as Mg is commonly correlated with strong zoning in the major components (i.e. the anorthite content). Variation in Mg diffusivity with plagioclase composition must be taken into account in modeling the profiles. Costa et al. (2003) suggested that the dependence of Mg diffusion on plagioclase composition was similar to that for Sr and other large cations – which exhibit strong increases in diffusivity with decreasing anorthite content – and was able to obtain good fits to natural Mg diffusion profiles in plagioclase phenocrysts by assuming that the relative dependence on composition of Mg diffusion was identical to that of Sr. However, as noted above, the compositional dependence of Mg diffusivity in plagioclase has not yet been investigated experimentally.

Here, we report the results of experiments to determine Mg diffusion coefficients in natural plagioclase crystals of a wide range of composition, from An<sub>93</sub> (anorthite) to An<sub>23</sub> (oligoclase), over a wide range of temperature extending downward to 800 °C. The experiments also address whether Mg chemical diffusion rates, which are relevant to the relaxation of Mg zoning profiles in plagioclase, may be different than Mg self-diffusion rates, which are relevant to <sup>26</sup>Al–<sup>26</sup>Mg resetting where the net flux of Mg among phases is negligible.

## 2. Experimental

The diffusion experiments were performed using natural single crystals of anorthite (An<sub>93</sub>), labradorite (An<sub>66</sub>), andesine (An<sub>43</sub>) and oligoclase (An<sub>23</sub>). Each crystal was oriented, sectioned with a low speed saw and mirror polished on one side, then placed in an open Pt capsule surrounded by a powder consisting of MgO, Al<sub>2</sub>O<sub>3</sub> and SiO<sub>2</sub> in 1:1:2 molar proportions, mechanically mixed in a 6:1 weight ratio with plagioclase powder of the same composition as the crystal. Two sets of experiments were performed, one with highly enriched <sup>25</sup>MgO in the powder source and the other with isotopically normal MgO. The experiments with <sup>25</sup>MgO provided better resolution in the measurement of the Mg diffusion profiles, and, as described below, allowed for a comparison between Mg self-diffusion coefficients (in experiments where there was a negligible net flux of Mg) and Mg chemical diffusion coefficients.

The open Pt capsule containing each crystal/powder diffusion couple was suspended in air within the hotspot of a 1 atm furnace and maintained at constant temperature, between 798 and 1150 °C, for times ranging from 25 min to 24 d. Following the experiment, the plagioclase single crystal was removed from the powder and rinsed in purified water and ethanol, mounted in epoxy with the polished surface exposed and coated with a 60 nm layer of gold, which provided a conductive surface layer for SIMS depth profiling analyses.

### 2.1. SIMS depth profiling analyses

Depth profiles of major elements (Na, Al, Si, and Ca) and Mg isotopes were performed using the WiscSIMS Cameca IMS-1280 ion microprobe at the University of Wisconsin-Madison (Valley and Kita, 2009; Kita et al., 2012). An O<sup>−</sup> primary ion beam was used, with total impact energy of 23 keV to the sample surface (−13 kV primary ion and +10 kV secondary ion acceleration voltages). The primary beam was focused to ~30 μm diameter with 30 nA intensity and raster size of 70 μm square, which leaves a sputtered crater that is flat over a ~40 μm square area. The field aperture was set to a 1600 μm square that restricted sampling to a central 20 μm square area on the sample surface (the magnification of the transfer lens was set to 80), with the beam position carefully adjusted at each analysis location so that only secondary ions produced from the center of the raster area were collected in the mass spectrometer. Mass resolution power was set to ~3000, high enough to separate interference peaks. The isotope peaks were detected by magnetic peak switching on the fixed axial detector (mono-collector), which is switchable between electron multiplier (EM) and Faraday Cup (FC), in the following order: <sup>23</sup>Na (2 s, EM), <sup>24</sup>Mg (10 s, EM), <sup>25</sup>Mg (10 s, EM), <sup>26</sup>Mg (10 s, EM), <sup>27</sup>Al (2 s, FC), <sup>28</sup>Si (2 s, FC), and <sup>40</sup>Ca (2 s, FC). A single cycle took ~54 s including waiting time to settle the magnetic field at each isotope. For the first set of samples, with natural Mg isotope abundances in the source powder, the minor Mg isotopes (<sup>25</sup>Mg and <sup>26</sup>Mg) were not included in the analysis and a single cycle took ~30 s. For a natural labradorite standard containing 0.1 wt% MgO (Lab1, An<sub>60</sub>; Kita et al., 2012), typical secondary ion intensities were 6 × 10<sup>4</sup> cps for <sup>23</sup>Na, 3000 cps for <sup>24</sup>Mg, 8 × 10<sup>5</sup> cps for <sup>27</sup>Al, 6 × 10<sup>5</sup> cps for <sup>28</sup>Si, and 4 × 10<sup>5</sup> cps for <sup>40</sup>Ca.

The secondary ions with higher initial energy were selected by using an energy offset (−50 V), similar to the conditions applied in previous diffusion profile studies (e.g., Ito and Ganguly, 2006). We note that this energy filtering was required to reduce molecular interferences for small radius ion microprobes, but not for the IMS-1280 which is capable of resolving interference peaks by applying high mass resolution power without losing secondary ion transmission. However, the sample surface becomes charged up to ~30 eV under our analytical conditions, which drastically changes the secondary ion intensity of low energy ions at the beginning of the depth profiling. The energy filtering method works well in keeping the secondary ion intensity relatively stable despite surface charging, with only a slight gradual decrease in ion counts with increasing depth over the first ~1 μm of sputtering. To correct for this small charging effect, Mg ion intensity at each depth is normalized to that of <sup>27</sup>Al. Thus, in experiments with isotopically normal MgO in the source materials, <sup>24</sup>Mg/<sup>27</sup>Al is used as a proxy for relative Mg concentration along the depth profile. Similarly, in experiments conducted with <sup>25</sup>Mg-enriched source materials, (<sup>24</sup>Mg + <sup>25</sup>Mg + <sup>26</sup>Mg)/<sup>27</sup>Al is used as a proxy for total Mg concentration, and the Mg isotope composition is recorded as <sup>25</sup>Mg/(<sup>24</sup>Mg + <sup>25</sup>Mg + <sup>26</sup>Mg).

Following SIMS depth profiling analyses, the sputtered pits were measured using a Zygo 3D optical surface profilometer. The central 20 μm square area of the pit that was sampled during the SIMS analysis was considered for depth measurement. The variation in depth within this central area was within 10–50 nm for each pit, compared to total depths between 1.26 and 9.57 μm, corresponding to a 2σ precision in depth measurement between 0.22% and 1.7% for each of the sputtered pits. The sputtering rate, for the beam conditions noted above, was found to be ~0.012–0.015 nm/s/nA, and increased slightly with the albite content of the plagioclase.

## 2.2. Diffusion profile fitting

To determine the diffusion coefficient, Mg elemental and  $^{25}\text{Mg}$  isotope concentration profiles were fit to the equation for one-dimensional diffusion in a semi-infinite medium with constant surface concentration (Crank, 1975):

$$\frac{C(x, t) - C_{surf}}{C_{init} - C_{surf}} = \text{erf} \frac{x}{2\sqrt{Dt}}. \quad (1)$$

Here,  $C$  represents the concentration at depth  $x$  after time  $t$ ,  $C_{surf}$  is the constant concentration at the crystal surface,  $C_{init}$  is the initial concentration within the crystal, and  $D$  is the diffusion coefficient. Eq. (1) was fit to each of the profiles by iteratively adjusting the fit parameters to minimize  $\chi^2$  using the Marquardt method. For the  $^{25}\text{Mg}$  concentration profiles,  $D$  and  $C_{surf}$  were the fit parameters, whereas the initial concentration in the plagioclase crystal ( $C_{init}$ ) was constrained to be the natural  $^{25}\text{Mg}$  isotopic abundance (0.100). For the Mg elemental concentration profiles,  $C_{init}$  was allowed to vary as an additional fit parameter. Although the variation in  $C_{init}$  was small among the different slabs of crystal used in the experiments, only a few percent in the case of labradorite, this variation was nevertheless significant compared to the small difference between  $C_{init}$  and  $C_{surf}$ . Hence, it was not possible to treat  $C_{init}$  as a constant for all experiments on a particular plagioclase composition. Fig. 1(a) shows an example of  $^{25}\text{Mg}$  concentration profile in labradorite, along with an error function curve showing the least squares fit of Eq. (1) to the data.

In many cases, a small amount of source material adhered to the polished surface following the diffusion anneal, distributed heterogeneously across the surface. Although care was taken to locate regions on the plagioclase surface that were as clean as possible for depth profiling, the upper portion of the depth profile often reflected contamination from the adhering source material. This type of surface contamination is commonly observed in SIMS depth profiles of diffusion experiments (e.g. Van Orman et al., 2001). The contaminated portion of the profile is obvious in an inverse error function plot, in which both sides of Eq. (1) are inverted through the error function (Fig. 1(b)). A kink in the inverted profile marks the transition from surface contamination to the actual diffusion profile, which is linear. Only the linear part of the profile beyond the kink is fitted to obtain  $D$ , as described above (Fig. 1(c)).

## 2.3. Error analysis

The formal uncertainty in  $D$  for each profile was estimated considering (1) the uncertainty in the depth of the sputtered pit and (2) the uncertainty due to scatter in the concentration along the diffusion profile. Propagating the error in the depth measurement is straightforward. Because  $D \propto x^2$ , the relative error in  $D$  from this source is simply double the relative error in the depth measurement. Determining the error due to scatter is more involved because the fitting function is not linear, and the fit parameters  $D$ ,  $C_{surf}$  and  $C_{init}$  exhibit some correlation. This error was determined from a contour plot of  $\chi^2$  with respect to  $D$  and  $C_{surf}$ , where the value of  $C_{init}$  (for Mg concentration profiles) was allowed to vary to minimize  $\chi^2$  for each pair of values of  $D$  and  $C_{surf}$  (e.g. Bevington and Robinson, 2002, Section 11.5). The standard deviation of  $D$  was taken to be the full range of the  $\Delta\chi^2 = 1$  contour, and this was combined with the error resulting from the depth measurement to provide an estimate of the formal uncertainty in each value of  $D$ .

A better measure of the overall error in determining the diffusion coefficients is their reproducibility in separate experiments

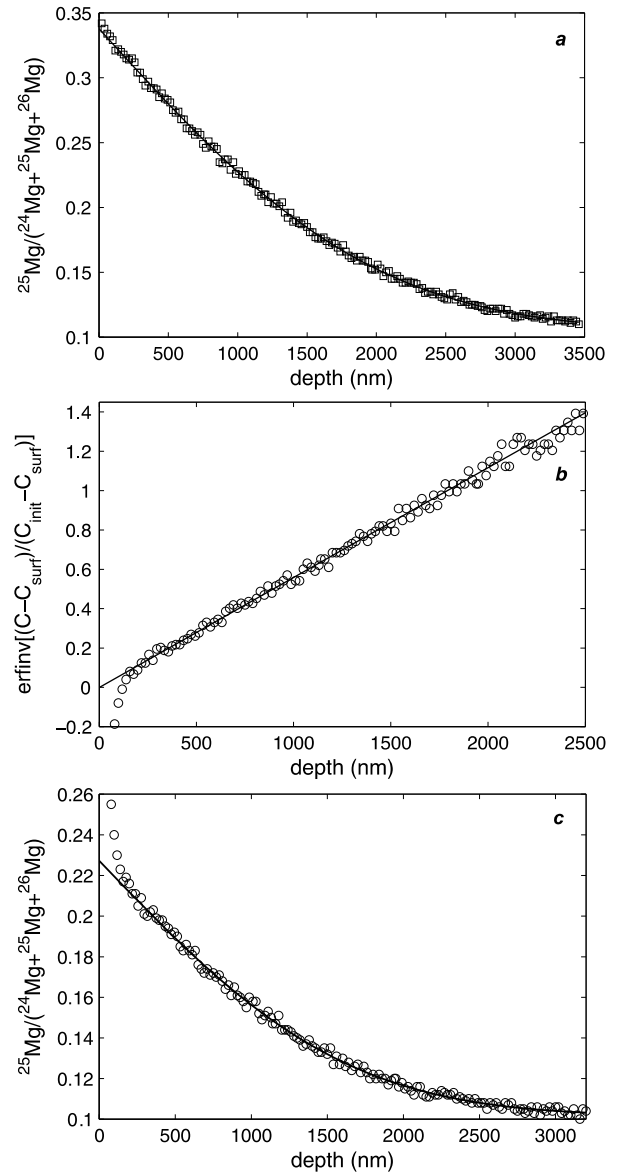


**Fig. 1.** Examples of Mg isotope diffusion profiles. (a) Profile without resolvable contamination from isotopically enriched powder retained on the mineral surface (Expt. MgLab16), with associated error function curve fit to the data. (b) Inverse error function plot of a profile that exhibits surface contamination (Expt. MgLab13). Only the linear portion of the profile beyond the kink is considered in fitting the data to obtain the diffusion coefficient. The same profile (Expt. MgLab13), uninverted, is shown in panel (c).

at similar conditions. For labradorite, three experiments were conducted at  $\sim 1050^\circ\text{C}$  and two at  $\sim 1150^\circ\text{C}$  to determine the diffusion coefficient in the  $c$  direction. The results of these experiments indicate that there are additional systematic errors not accounted for in the formal error analysis, which are on the order of 12% in  $D$  at both temperatures. The origin of this scatter beyond the formal uncertainty limits is not known, but it is nonetheless important to include when evaluating the errors on the Arrhenius parameters, and on the compositional dependence of Mg diffusivity. In estimating the overall uncertainty in  $D$  for each experiment, we assume that the systematic error is uncorrelated with the formal error estimate, and that it has the same relative value (12%) for each experiment. This overall estimate, rather than the formal uncertainty, was used in the weighted linear regressions discussed below, and yields values of reduced chi-square that are close to the expected value of unity in most cases.

**Table 1**  
Experimental conditions and results.

Expt. ID	T (°C)	Time (s)	Orientation*	Composition	<sup>25</sup> Mg tracer?	D (m <sup>2</sup> /s)	log D	σ formal	σ total
MgAnor1	1150	1.08 × 10 <sup>4</sup>	(010)	An <sub>93</sub>	No	3.41 × 10 <sup>-17</sup>	-16.47	0.02	0.07
MgAnor3	1050	8.28 × 10 <sup>4</sup>	(010)	An <sub>93</sub>	No	8.03 × 10 <sup>-18</sup>	-17.10	0.01	0.06
MgAnor5	898	1.13 × 10 <sup>6</sup>	(010)	An <sub>93</sub>	Yes	2.54 × 10 <sup>-19</sup>	-18.60	0.02	0.07
MgAnor6	1000	1.62 × 10 <sup>5</sup>	(010)	An <sub>93</sub>	Yes	3.35 × 10 <sup>-18</sup>	-17.47	0.03	0.08
MgLab3-1	1149	1.50 × 10 <sup>3</sup>	(001)	An <sub>67</sub>	No	2.43 × 10 <sup>-16</sup>	-15.61	0.08	0.14
MgLab3-2	"	"	"	"	"	2.38 × 10 <sup>-16</sup>	-15.62	0.03	0.08
MgLab4	1101	3.00 × 10 <sup>3</sup>	(001)	An <sub>67</sub>	No	1.23 × 10 <sup>-16</sup>	-15.91	0.06	0.11
MgLab5	1053	7.20 × 10 <sup>3</sup>	(001)	An <sub>67</sub>	No	5.08 × 10 <sup>-17</sup>	-16.29	0.04	0.09
MgLab7	1002	2.34 × 10 <sup>4</sup>	(001)	An <sub>67</sub>	No	2.33 × 10 <sup>-17</sup>	-16.63	0.07	0.13
MgLab10	1150	1.08 × 10 <sup>4</sup>	(001)	An <sub>67</sub>	No	3.26 × 10 <sup>-16</sup>	-15.49	0.02	0.07
MgLab11	1050	8.28 × 10 <sup>4</sup>	(001)	An <sub>67</sub>	No	6.47 × 10 <sup>-17</sup>	-16.19	0.02	0.07
MgLab13	900	5.90 × 10 <sup>5</sup>	(001)	An <sub>67</sub>	Yes	1.40 × 10 <sup>-18</sup>	-17.85	0.02	0.08
MgLab15	950	2.48 × 10 <sup>5</sup>	(001)	An <sub>67</sub>	Yes	3.67 × 10 <sup>-18</sup>	-17.44	0.02	0.07
MgLab17	798	2.06 × 10 <sup>6</sup>	(001)	An <sub>67</sub>	Yes	6.13 × 10 <sup>-20</sup>	-19.21	0.04	0.09
MgLab19	1047	3.60 × 10 <sup>4</sup>	(001)	An <sub>67</sub>	Yes	6.68 × 10 <sup>-17</sup>	-16.18	0.04	0.09
MgLab14	899	6.01 × 10 <sup>5</sup>	(010)	An <sub>67</sub>	Yes	1.20 × 10 <sup>-18</sup>	-17.92	0.03	0.08
MgLab16	998	8.28 × 10 <sup>4</sup>	(010)	An <sub>67</sub>	Yes	1.51 × 10 <sup>-17</sup>	-16.82	0.01	0.07
MgLab20	1047	3.60 × 10 <sup>4</sup>	(010)	An <sub>67</sub>	Yes	3.56 × 10 <sup>-17</sup>	-16.45	0.02	0.07
MgAnd2	1048	1.80 × 10 <sup>4</sup>	(001)	An <sub>43</sub>	Yes	4.37 × 10 <sup>-16</sup>	-15.36	0.01	0.06
MgAnd3	850	6.88 × 10 <sup>5</sup>	(001)	An <sub>43</sub>	Yes	4.72 × 10 <sup>-18</sup>	-17.33	0.04	0.09
MgOl1	799	5.98 × 10 <sup>5</sup>	(001)	An <sub>23</sub>	Yes	1.72 × 10 <sup>-18</sup>	-17.76	0.09	0.14
MgOl2	852	9.72 × 10 <sup>4</sup>	(001)	An <sub>23</sub>	Yes	3.08 × 10 <sup>-17</sup>	-16.51	0.05	0.10
MgOl3	900	2.88 × 10 <sup>4</sup>	(001)	An <sub>23</sub>	Yes	5.72 × 10 <sup>-17</sup>	-16.24	0.05	0.11
MgOl4	951	1.08 × 10 <sup>4</sup>	(001)	An <sub>23</sub>	Yes	1.01 × 10 <sup>-16</sup>	-16.00	0.09	0.14

\* Indicates diffusion normal to the listed crystallographic plane.

### 3. Results

The diffusion coefficients determined in each experiment are listed in Table 1. In experiments that utilized a <sup>25</sup>Mg tracer, the diffusion coefficients determined from the ΣMg/Al and <sup>25</sup>Mg/ΣMg concentration profiles were found to be in good agreement, but the <sup>25</sup>Mg/ΣMg concentration profile was generally much better resolved and yielded a more precise value of the diffusion coefficient. The diffusion coefficients obtained from the <sup>25</sup>Mg/ΣMg profile are considered more reliable, and these are the values reported in Table 1 for the isotope tracer experiments.

#### 3.1. Mg chemical diffusion vs. self-diffusion

The chemical diffusion coefficient and self-diffusion coefficient are related by (e.g. Shewmon, 1989, Section 4.4):

$$D_{Mg} = D_{Mg}^* (1 + d \ln \gamma_{Mg} / d \ln x_{Mg}), \quad (2)$$

where  $D_{Mg}$  is the intrinsic chemical diffusion coefficient,  $D_{Mg}^*$  is the self-diffusion coefficient that would be measured in a system where no chemical concentration gradient is present,  $\gamma_{Mg}$  is the activity coefficient and  $x_{Mg}$  is the molar concentration. In general, the diffusion coefficient obtained from a chemical diffusion profile is an interdiffusion coefficient that depends upon the fluxes and molar volumes of at least two chemical species (e.g. Balluffi, 1960). However, in the present case, where Mg is present at very low concentrations, and diffuses relatively rapidly, the interdiffusion coefficient is approximately equal to the intrinsic chemical diffusion coefficient, and it is reasonable to assume that the values of  $D$  obtained from chemical concentration profiles are equal to the intrinsic  $D_{Mg}$  within error. The term in parentheses in Eq. (2), often referred to as the thermodynamic factor, is equal to one in the case of an ideal or dilute (Henry's Law) solution. Hence, if Mg in plagioclase is sufficiently dilute to be in the Henry's Law regime, the chemical and self-diffusion coefficients will be equal.

In all of the experiments with anorthite, andesine, and oligoclase, and in experiments with labradorite at temperatures of 1000 °C and greater, there was a net flux of Mg from the source material to the plagioclase. Therefore, most of the experiments

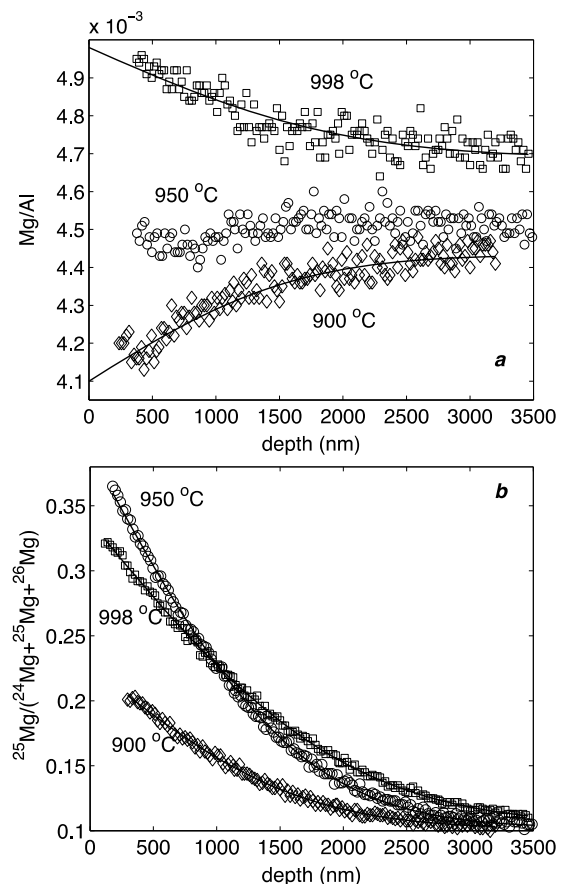


**Fig. 2.** Diffusion profiles from experiments MgLab13 (diamonds), MgLab15 (circles), and MgLab16 (squares). The curves shown through the Mg/Al profiles in (a) use the diffusion coefficient determined by fitting the isotope profile from the same experiment, as shown in (b). The Mg concentration and isotopic profiles are consistent with the same diffusion coefficient, whether the chemical and isotopic fluxes are in the same direction or opposite.

measured chemical diffusion coefficients rather than self-diffusion coefficients. However, as shown in Fig. 2, at  $\sim 950^\circ\text{C}$  there was no resolvable flux of Mg between labradorite and the source material, and at lower temperatures there was a net flux of Mg out of the labradorite crystal (the solubility of Mg in plagioclase increases with temperature, and evidently the specimen used in these experiments is saturated with Mg at  $\sim 950^\circ\text{C}$ ). Because there is no resolvable flux of Mg in the  $950^\circ\text{C}$  experiment – only an exchange of Mg isotopes – this experiment is effectively a self-diffusion experiment.

Fig. 2 shows Mg concentration profiles from three experiments with labradorite at  $998^\circ\text{C}$ ,  $950^\circ\text{C}$  and  $900^\circ\text{C}$ , along with isotopic concentration profiles from the same experiments. The model curves fit to the Mg/Al profiles did not treat the diffusion coefficient as a free parameter, but instead were generated using the diffusion coefficient determined by fitting the isotopic concentration profile from the same experiment. It can be seen that the Mg/Al and Mg isotope profiles are consistent with the same diffusion coefficient, whether the chemical concentration gradient is in the same direction or opposite to the isotopic concentration gradient. The diffusion coefficient obtained from the Mg isotope profile in the  $950^\circ\text{C}$  experiment, which can be considered a self-diffusion coefficient because there is no significant chemical gradient, is in agreement with the chemical diffusion coefficient interpolated to this temperature. The interpolated chemical diffusion coefficient at  $950^\circ\text{C}$ , based on a weighted regression of Mg chemical diffusion data for labradorite in the (001) direction, is  $3.62 \times 10^{-18} \text{ m}^2/\text{s}$ , which is within error of the Mg self-diffusion coefficient of  $3.67 \pm 0.26 \times 10^{-18} \text{ m}^2/\text{s}$ . This suggests that the chemical and self-diffusion coefficients are equal in these experiments, and that the Mg concentrations in labradorite are in the Henry's Law regime. The Mg concentrations in the other plagioclase samples are lower than in labradorite, and it is therefore likely that these experiments were also conducted in the Henry's Law regime. As shown below, the chemical diffusion coefficients for anorthite determined in this study are in good agreement with the self-diffusion coefficients determined by LaTourrette and Wasserburg (1998), providing further support for the equivalence of chemical and self-diffusion coefficients for Mg in plagioclase.

It is important to note, however, that in natural situations Mg may diffuse not only in response to its own concentration gradient but also in response to gradients in major element concentrations (Costa et al., 2003). The activity of Mg depends on the anorthite content of the plagioclase, and zoning in anorthite content will therefore have a strong influence on the flux of Mg. Because CaAl–NaSi interdiffusion (Grove et al., 1984) is many orders of magnitude slower than diffusion of Mg in plagioclase, a gradient in Mg concentration may be preserved in plagioclase crystals that are zoned in major elements, on timescales much longer than those relevant to Mg diffusion. This is not due to a direct diffusive coupling between Mg and any of the major elements, but rather to the influence of the major elements on Mg activity. The major element gradient does not affect the diffusivity of Mg, but rather affects the driving force – the chemical potential gradient (Costa et al., 2003). Magnesium diffuses rapidly enough that it may effectively “partition” along the major element zoning profile in plagioclase. This type of diffusional flux coupling is also commonly observed in silicate melts (e.g. Watson, 1982; Zhang et al., 1989). In the presence of major element zoning, gradients in Mg concentration may persist during heating events that are sufficient to homogenize Mg isotopes. In the absence of major element zoning, our experimental results indicate that gradients in Mg elemental concentration will be relaxed at the same rate as gradients in Mg isotopic composition. The diffusion coefficients reported in this paper are directly applicable to Mg isotope diffusion in plagioclase, and to Mg chemical diffusion when only a gradient

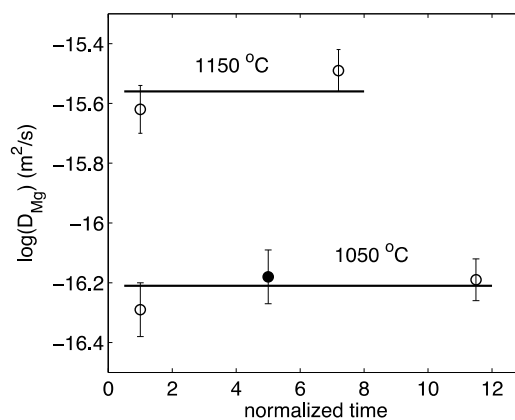


Fig. 3. Diffusion coefficients determined from experiments at 1150 and  $1050^\circ\text{C}$ , plotted against the anneal time (normalized to the duration of the shortest experiment in the series). The diffusion coefficients determined from experiments that vary in duration by an order of magnitude agree within  $\sim 20\%$ . Open circles: diffusion coefficients obtained from chemical (Mg/Al) concentration profiles; closed circle: diffusion coefficient obtained from  $^{25}\text{Mg}/\Sigma\text{Mg}$  isotopic concentration profile.

in Mg concentration exists. For Mg chemical diffusion in the presence of major element zoning, it is necessary to account for the influence of the zoning on the chemical potential gradient of Mg, as discussed for example by Costa et al. (2003).

### 3.2. Time series

Fig. 3 shows the results experiments performed for different durations at  $\sim 1050^\circ\text{C}$  and  $\sim 1150^\circ\text{C}$ . Both sets of experiments examined Mg diffusion in labradorite normal to (001). The diffusion coefficients are reproducible within  $\sim 20\%$  relative for experiments ranging in duration over more than a factor of ten.

### 3.3. Anisotropy

A few experiments were performed as a preliminary investigation of anisotropy in the diffusion of Mg in labradorite (Table 1). Diffusion appears to be slightly slower normal to (010) than normal to (001), in experiments conducted under the same conditions, but the difference is barely resolvable. At  $1047^\circ\text{C}$ , two experiments (MgLab19 and MgLab20) were performed simultaneously under the same conditions, and these yield  $D_{(001)}/D_{(010)} = 2.24 \pm 0.59$ . In experiments performed separately at similar temperatures of  $\sim 1000^\circ\text{C}$  and  $\sim 900^\circ\text{C}$ , the same diffusivity ratio is  $1.41 \pm 0.46$  and  $1.14 \pm 0.29$ , respectively (after making a small correction to compare the diffusion coefficients at the same temperature).

LaTourrette and Wasserburg (1998) found similar anisotropy for Mg diffusion in anorthite. Based on their data we can calculate the ratio  $D_{(001)}/D_{(010)}$ , which is  $2.8 \pm 1.6$  at  $1400^\circ\text{C}$  and  $2.5 \pm 1.4$  at  $1300^\circ\text{C}$ .

Considering the available data, which indicates that anisotropy between the *b* and *c* directions is weak in both labradorite and anorthite, it is probably adequate for most applications to treat Mg diffusion in plagioclase as isotropic.

### 3.4. Temperature and compositional dependence

The diffusion coefficients determined from each experiment are shown on Arrhenius plots in Fig. 4. In Fig. 4(a) the data for each plagioclase composition (and for each crystallographic orientation, in the case of labradorite) are fit separately to the Arrhenius equation:

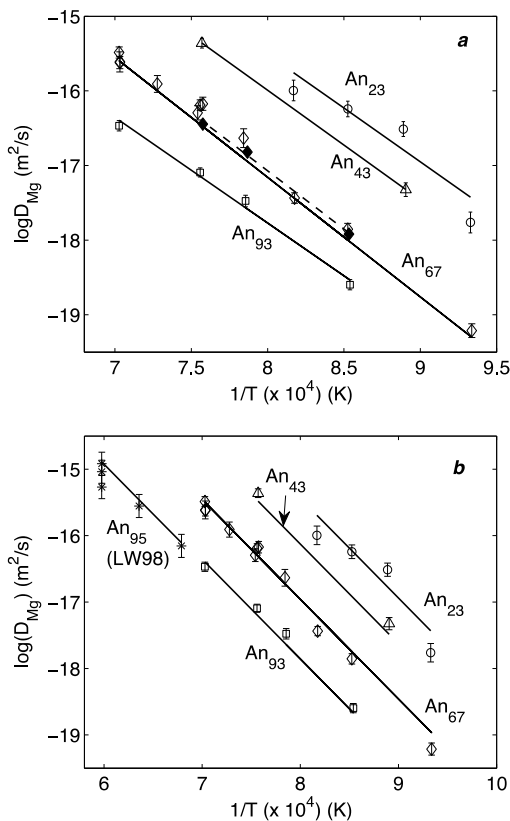


**Fig. 4.** Arrhenius plots showing the dependence of Mg diffusion coefficients on temperature and plagioclase composition. In (a) the data for each plagioclase composition (and crystallographic orientation, for labradorite) are fit individually. In (b) the data set as a whole is fit to a single Arrhenius-type equation, where the logarithm of the pre-exponential factor is a linear function of the anorthite content of the plagioclase (see text for details). Squares – anorthite (An<sub>93</sub>); open diamonds – labradorite (An<sub>67</sub>) normal to (001); filled diamonds – labradorite (An<sub>67</sub>) normal to (010); triangles – andesine (An<sub>43</sub>); circles – oligoclase (An<sub>23</sub>); asterisks – anorthite (An<sub>95</sub>) normal to (010), from LaTourrette and Wasserburg (1998).

$$\ln D = \ln D_0 - \frac{Q}{RT} \quad (3)$$

where  $D_0$  is the pre-exponential factor,  $Q$  is the activation energy,  $R$  is the gas constant and  $T$  is temperature in K. Values of the pre-exponential factor and activation energy determined from each fit are listed in Table 2.

It can be seen that the diffusion coefficients are strongly correlated with plagioclase composition, increasing systematically with decreasing anorthite content. A similar increase in diffusivity in more sodic plagioclase has been observed for many other cations in plagioclase, including Sr, Pb, Ba, Nd and Ca (Behrens et al., 1990; Cherniak, 1995, 2002, 2003, 2010; Cherniak and Watson, 1992, 1994; Giletti and Casserly, 1994; LaTourrette and Wasserburg, 1998). We found that the data for Mg diffusion in plagioclase, including the data of LaTourrette and Wasserburg (1998) for An<sub>95</sub>, could be fit reasonably well ( $\chi^2_{reduced} = 2.88$ ) by considering the activation energy to be constant, and the logarithm of the pre-

exponential factor to be a linear function of the anorthite content,  $x_{An}$  (Fig. 4(b)):

$$\ln D = (-6.06 \pm 1.10) - (7.96 \pm 0.42)x_{An} - \frac{287 \pm \text{kJ/mol}}{RT}, \quad (4)$$

where the uncertainties are  $2\sigma$  and  $D$  is in  $\text{m}^2/\text{s}$ . The data set was fit by minimizing  $\chi^2$ , and the uncertainties were estimated from  $\chi^2$  contour plots, in the manner described above for the fitting of the diffusion profiles, with  $2\sigma$  reflecting the full range of the  $\Delta\chi^2 = 4$  contour. We also examined models in which the activation energy was a function of composition (with or without the pre-exponential factor also being a function of composition), but these yielded poorer fits to the data. Eq. (4) is of the same form as the equation proposed by Costa et al. (2003) to describe Mg diffusivity in plagioclase, which is based on the compositional dependence observed experimentally for Sr diffusion. The Costa et al. (2003) expression can be written as  $\ln D = -6.07 - 9.44x_{An} - 266 \text{ (kJ/mol)}/(RT)$ ; compared to our Eq. (4), this expression has a stronger compositional dependence and weaker temperature dependence. The Costa et al. (2003) preliminary estimate yields Mg diffusivities similar to ours for anorthite at high temperature, but over-predicts the diffusivities at lower temperatures and lower anorthite contents (Fig. 5). For albite at  $850^\circ\text{C}$ , the discrepancy is a factor of 10. Magma transfer timescales inferred from Mg zoning profiles in plagioclase using the Costa et al. (2003) expression may therefore need to be adjusted upward significantly. For example, the magma transfer timescales inferred by Druitt et al. (2012) for the Minoan caldera-forming eruption at Santorini are based on Mg diffusion profiles in plagioclase phenocrysts with  $\sim\text{An}_{30}\text{--An}_{90}$ , which are considered to have been developed primarily at  $900^\circ\text{C}$ . At this temperature and these plagioclase compositions, the Costa et al. (2003) expression used by Druitt et al. (2012) over-estimates the Mg diffusivities by a factor of 2.25–5.5 relative to our results. The magma transfer timescales estimated by Druitt et al. (2012) may therefore need to be revised upward by a similar factor.

## 4. Discussion

### 4.1. Diffusion mechanism

It appears that  $D_0$ , but not  $Q$ , varies systematically with plagioclase composition, both for Mg (this study) and Sr (Giletti and Casserly, 1994). This suggests that the variation in diffusivity with composition is due to systematic changes in the defect population, rather than to changes in the migration energy, as the composition varies between anorthite and albite. It is well known that plagioclase can incorporate excess  $\text{Si}^{4+}$  in tetrahedral sites, which are charge-compensated by the formation of vacancies on the large cation A sites that are normally occupied by  $\text{Na}^+$  and  $\text{Ca}^{2+}$  (e.g. Longhi and Hays, 1979). The incorporation of excess  $\text{SiO}_2$  may therefore lead to an enhancement in the diffusivity of cations that diffuse by means of site exchanges with vacancies on the A-sites (Behrens et al., 1990). A recent study by Faak et al. (2013) indicates that the diffusivity of Mg in labradorite increases with increasing silica activity, which suggests that vacancies created to compensate

**Table 2**  
Arrhenius parameters.

Crystal	Composition	$\log D_0$	$2\sigma$	Q (kJ/mol)	$2\sigma$	$\chi^2_{reduced}$ (MSWD)
Anorth	An <sub>93</sub>	−6.45	1.02	271	25	1.89
Lab (001)	An <sub>67</sub>	−4.33	0.62	307	15	1.75
Lab (010)	An <sub>67</sub>	−4.60	1.82	298	44	0.72
Olig	An <sub>43</sub>	−4.23	1.39	282	33	8.07
And	An <sub>23</sub>	−3.99	2.77	276	61	n.d.

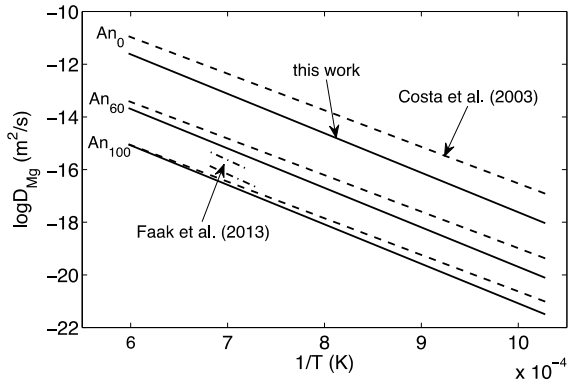


**Fig. 5.** Comparison of Mg diffusion coefficients from this work (solid lines, Eq. (4)) with those from the model of Costa et al. (2003) (dashed lines) and those from the experiments of Faak et al. (2013) (dash-dot lines). The Faak et al. (2013) data shown here were acquired on An<sub>60</sub> plagioclase, under both SiO<sub>2</sub>-saturated conditions (plagioclase in contact with Cpx + SiO<sub>2</sub>, upper line), and SiO<sub>2</sub>-undersaturated conditions (with Cpx only, lower line).

the charge of excess Si<sup>4+</sup> play a significant role in Mg diffusion. Analysis of our diffusion source powders after the experiments reveals the presence of silica, indicating that our experiments were conducted under silica-saturated conditions. Hence, the compositional dependence found in our study cannot be explained in terms of systematic variations in silica activity with anorthite/albite content among the different plagioclase crystals used. It is also problematic to explain the rapid Mg diffusivities in andesine and oligoclase solely in terms of higher vacancy concentrations, because the vacancy concentrations required are implausibly large based on those inferred for silica-saturated labradorite by Faak et al. (2013).

#### 4.2. Thermal resetting of <sup>26</sup>Al–<sup>26</sup>Mg ages

The relative age recorded as excess <sup>26</sup>Mg in plagioclase found in meteorites may be reset due to diffusive exchange of Mg isotopes between the plagioclase crystal and its surroundings. Al-rich chondrules in unequibrated ordinary chondrites studied by Russell et al. (1996) show <sup>26</sup>Al relative ages from ~2 Ma to more than 5 Ma after CAI, which was originally interpreted as an extended nebular time scale. Huss et al. (2001) later suggested that radiogenic <sup>26</sup>Mg excess in plagioclase in many of these chondrules were redistributed by mild thermal metamorphism in the parent asteroid. Chondrules within the least altered, least metamorphosed chondrites record <sup>26</sup>Al relative ages mostly ~2 Ma after CAI formation without significant variations (0.5–1 Ma at most), though many chondrules in CR chondrites show younger ages more than 3 Ma after CAIs (e.g., Hutcheon et al., 2009; Nagashima et al., 2007; 2008; Tenner et al., 2013). It is critical to evaluate whether these ages are primary, and thus reflect an extended period of chondrule formation within the early solar system, or whether the age dispersion may reflect variable resetting during later thermal events.

High precision ion microprobe analyses of anorthite-rich plagioclase in CAIs provide the best possible time resolution on the relative <sup>26</sup>Al–<sup>26</sup>Mg ages at a scale better than 10 ka, as indicated from well-correlated <sup>26</sup>Al–<sup>26</sup>Mg isochron data from Leoville (CV3) type B1 CAI (Kita et al., 2012). However, radiogenic <sup>26</sup>Mg in plagioclase in CAIs is easily disturbed by thermal metamorphism in the parent body. For example, MacPherson et al. (2012) showed a well-correlated <sup>26</sup>Al–<sup>26</sup>Mg isochron from melilite, fassaite, and spinel in type B CAI in Vigarano (CV3), while <sup>26</sup>Mg excess in plagioclase of the same CAI was lost and exchanged with spinel included in plagioclase. Potential magnesium diffusion of plagioclase during

mild thermal resetting is very important for the interpretation of chronological data.

We first treat the case of a transient heating event, and address the duration of heating that is required, at various temperatures, to alter the <sup>26</sup>Al/<sup>26</sup>Mg age. For simplicity, the heating event is considered here to be isothermal, and to occur after all <sup>26</sup>Al has decayed. The mineral assemblage is considered to consist of plagioclase (as the sole high Al/Mg phase) and a low Al/Mg phase such as olivine or pyroxene. This assemblage is common in chondrules, and is the basis for most <sup>26</sup>Al ages determined using internal isochrons (Kita and Ushikubo, 2012). Thermal resetting in this system depends significantly only on the diffusion of Mg in plagioclase, if the low Al/Mg phase provides an effectively infinite sink for <sup>26</sup>Mg. However, it is possible for the low Al/Mg phase to exert an influence on thermal resetting if Mg diffusivity in this phase is very slow relative to plagioclase. We performed numerical simulations to examine the conditions under which the low Al/Mg phase may affect thermal resetting, using the finite difference model developed by Van Orman et al. (2006). The low Al/Mg phase was considered to exert a significant influence if it shifted the Al–Mg age by 10% or more relative to the infinite sink case. For mineral grains all of the same size, this was found to be the case only if

$$\log \frac{D}{D^{plag}} < 2 + 2 \log \frac{\phi^{plag}}{\phi} K_{Mg}, \quad (5)$$

where  $\phi$  and  $\phi^{plag}$  represent the proportions of the low Al/Mg phase and the plagioclase, respectively, and  $K_{Mg}$  is the partition coefficient between plagioclase and the low Al/Mg phase. This log-linear relationship holds for  $\frac{\phi^{plag}}{\phi} K_{Mg} < 0.05$ , which is likely to apply in practically all cases given the low solubility of Mg in plagioclase and the relative abundance of Mg-rich phases in chondrites, chondrules and CAIs.

We evaluated Eq. (5) for the case of plagioclase exchanging Mg isotopes with olivine, using Mg self-diffusion data for San Carlos olivine (Chakraborty et al., 1994) and Mg partitioning data from Faak et al. (2013). The Faak et al. (2013) partitioning data apply to plagioclase in equilibrium with clinopyroxene; we assume that the solubility of Mg in plagioclase follows the same relationship in the presence of olivine and orthopyroxene (the common chondrule assemblage), and that the silica activity follows the forsterite–enstatite buffer. We also assume that olivine and plagioclase are present in similar proportions. Under these conditions, we find that olivine provides an effectively infinite sink for Mg isotopes produced within plagioclase at all temperatures that are likely to be relevant to late thermal processing of chondrules. The most extreme case is for albite, where Mg diffusion in olivine is a factor of ~10<sup>4</sup> slower than in the plagioclase. Even in this case, however, Mg has sufficiently low solubility in plagioclase, at temperatures less than 1000 °C, that olivine provides an effectively infinite sink for Mg isotopes. For An<sub>60</sub> plagioclase, as another example, olivine provides an infinite sink below 1330 °C.

Where an infinite sink exists, the fractional loss  $f$  of excess <sup>26</sup>Mg from spherical plagioclase grains during an isothermal heating event is given by Crank (1975), Eq. (6.20):

$$f = 1 - \frac{6}{\pi^2} \frac{1}{n^2} \exp(-n^2 \pi^2 D_{Mg} t / a^2), \quad (6)$$

where  $t$  is the isothermal heating time and  $a$  is the radius of the plagioclase. The system considered here is a simple two-point isochron system where the relative age is controlled by plagioclase. Diffusional loss of half of the excess <sup>26</sup>Mg ( $f = 0.5$ ) from plagioclase is equivalent to a change in the isochron age of one half-life,  $f = 0.75$  is equivalent to a change of two half-lives, and so on, i.e.:

$$\Delta t_{Al-Mg} = \ln(1 - f) / \lambda, \quad (7)$$

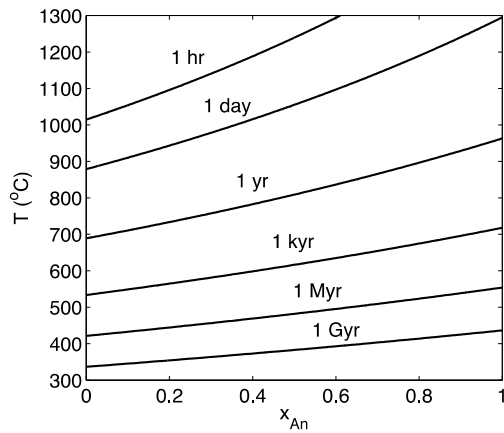


**Fig. 6.** Contour plot showing the heating time required to reset the  $^{26}\text{Al}$ – $^{26}\text{Mg}$  age by one half-life (705 000 yr), for plagioclase crystals 25  $\mu\text{m}$  in radius. The diffusion coefficients used in the calculations were obtained using Eq. (4). The time required for complete resetting (5 half-lives) is a factor of 10 longer than shown here. The time required for the minimum detectable resetting (defined here as a change of 40 000 yr in the  $^{26}\text{Al}$ – $^{26}\text{Mg}$  age) is a factor of  $\sim 230$  less than shown in the figure.

where  $\lambda$  is the  $^{26}\text{Al}$  decay constant. Note that diffusive loss of  $^{26}\text{Mg}$  from the plagioclase results in a younger apparent age, and  $\Delta t_{\text{Al-Mg}}$  represents the amount by which the recorded age has decreased due to the thermal event. Combining Eqs. (6) and (7), the heating time  $t$  required to alter the apparent age by a given amount can be calculated. A useful measure of the heating time required to significantly alter the  $^{26}\text{Al}$ – $^{26}\text{Mg}$  system in plagioclase is that required to alter the  $^{26}\text{Al}$  age by one half-life ( $\sim 705\,000$  yr), which is given by  $t_{\text{alter}} = 0.0306a^2/D_{\text{Mg}}$ . The heating time required for complete resetting – defined here as a change in the age of 5 half-lives – is a factor of 10 longer, i.e.  $t_{\text{reset}} = 0.31a^2/D_{\text{Mg}}$ . The heating time required for minimum detectable resetting – defined here as a change in the age of 40 ka – is only  $1.32 \times 10^{-4}a^2/D_{\text{Mg}}$ . Fig. 6 shows a contour plot of the heating time ( $t_{\text{alter}}$ ) required to reset the  $^{26}\text{Al}$ – $^{26}\text{Mg}$  isochron age by one half-life for plagioclase grains 25  $\mu\text{m}$  in radius, as a function of temperature and plagioclase composition.

At high temperatures near the plagioclase solidus, heating times on the order of an hour to a day are sufficient to effect significant loss of excess  $^{26}\text{Mg}$  from 50  $\mu\text{m}$  diameter plagioclase grains. Fine-grained plagioclase in CAIs or chondrules may be significantly reset by short ( $\sim$ month to year) near-solidus heating events resulting from nebular shock waves (Desch et al., 2002). Larger anorthite crystals in CAIs require much longer heating times; for millimeter-sized grains, the resetting time is on the order of 100 years at near-solidus temperatures.

Thermal resetting during internal heating of the parent body is also likely for all but the least metamorphosed chondrites. Only at temperatures below  $\sim 400$ – $450$  °C can fine-grained plagioclase grains escape thermal resetting on timescales of tens of millions of years.

For objects that experienced prolonged heating within a parent body, the  $^{26}\text{Al}$ – $^{26}\text{Mg}$  dates recorded by plagioclase may reflect closure of the system during slow cooling. The closure temperature is the temperature at which plagioclase effectively becomes closed to  $^{26}\text{Mg}$  diffusive loss, and corresponds to the temperature along the cooling path that the  $^{26}\text{Al}$ – $^{26}\text{Mg}$  age records. If the initial temperature is sufficiently high, the closure temperature model developed by Dodson (1973) can be used to calculate the closure temperature; a more general model was developed by Ganguly and Tirone (1999) that is valid for arbitrarily small diffusive losses during cooling, and we present the results of both models here. Both the Dodson (1973) and Ganguly and Tirone (1999) models assume continuous cooling, with an effectively infinite sink for daughter

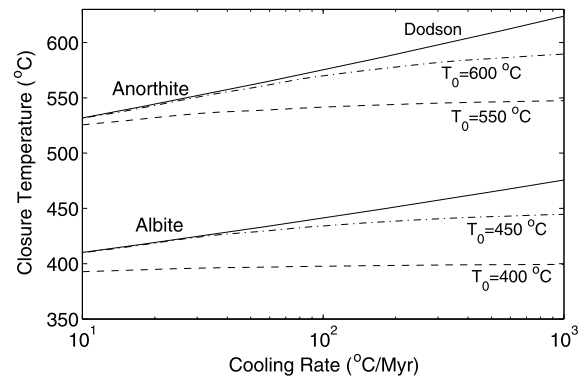


**Fig. 7.** Closure temperatures for plagioclase end-members anorthite and albite calculated using the Dodson (1973) model (solid curves), and the Ganguly and Tirone (1999) model (dashed and dash-dot curves) for different initial temperatures. All calculations apply to spherical plagioclase grains 25  $\mu\text{m}$  in radius. The Arrhenius parameters used in the calculations were obtained from Eq. (4).

products outside the crystal of interest. Closure temperatures for the  $^{26}\text{Al}$ – $^{26}\text{Mg}$  system in anorthite and albite are shown in Fig. 7, as a function of cooling rate for grain radii of 25  $\mu\text{m}$ . The calculated closure temperature of albite-rich plagioclase is up to 150 °C lower than that of anorthite, which translates to an age difference of up to  $\sim 5$  Ma for albite-rich plagioclase relative to anorthite at a cooling rate of 30 °C/Ma.

From ion microprobe measurements of the magnesium isotope compositions of plagioclase grains in two H4 chondrites, Zinner and Göpel (2002) determined ages of  $5.4 \pm 0.1$  and  $6.1 \pm 0.2$  Ma after CAIs, for San Marguerite and Forest Vale meteorites, respectively. Most of the plagioclase grains studied were reported to have grain sizes of  $\sim 50$   $\mu\text{m}$  and compositions in the range  $\text{An}_{15}$ – $\text{An}_{55}$ . Various mineralogical thermometers give consistent results for H4 chondrites, indicating peak metamorphic temperatures of  $\sim 750$  °C (Ganguly et al., 2013). At this temperature, excess  $^{26}\text{Mg}$  would be lost rapidly from the H4 plagioclase grains, with complete resetting requiring only on the order of a decade. Because the various mineralogical thermometers applied to H4 chondrites require much longer times to equilibrate at the recorded temperatures, it is clear that any excess  $^{26}\text{Mg}$  that had accumulated in the plagioclase prior to heating within the H chondrite parent body must have been lost at peak metamorphic temperatures, and that the  $^{26}\text{Al}/^{26}\text{Mg}$  ages therefore record closure during cooling.

For plagioclase grains 25  $\mu\text{m}$  in radius with compositions  $\text{An}_{15}$ – $\text{An}_{55}$ , the closure temperatures for Mg are  $449 \pm 23$ ,  $484 \pm 25$ , and  $523 \pm 28$  °C, for cooling rates of 10, 100 and 1000 °C/Myr, respectively. The Mg closure temperatures are similar to those for Pb in 50–130  $\mu\text{m}$  diameter phosphates (Göpel et al., 1994) at the same cooling rates, which are  $456 \pm 17$ ,  $501 \pm 20$  and  $551 \pm 22$  °C, respectively (using the Arrhenius parameters for Pb diffusion in apatite of Cherniak et al., 1991). Zinner and Göpel (2002) argued that the relative Al–Mg ages of plagioclase separated from two H4 chondrites, San Marguerite and Forest Vale, are consistent with their phosphate Pb–Pb ages, which are  $4562.7 \pm 0.6$  Ma and  $4560.9 \pm 0.7$  Ma, respectively (Göpel et al., 1994), relative to those of CAIs ( $4567.2 \pm 0.6$  Ma using the value of Amelin et al., 2002). More recently, the absolute Pb–Pb ages of CAIs have been revised for the effect of uranium isotope fractionation (e.g., Amelin et al., 2010; Brennecka et al., 2010; Connelly et al., 2012), and phosphate Pb–Pb ages need to be re-evaluated. However, relative Pb–Pb ages between H4 phosphates may not change more than 1–2 Ma, and thus the overall similarity between Al–Mg ages and Pb–Pb ages are consistent with their coeval closure during the same cooling event.

The difference in closure temperature between anorthite-rich plagioclase and albite-rich plagioclase raises some concerns about the potential time difference between FeO-rich chondrules

and Mg-rich chondrules in CO3.05 chondrite Y-81020, because most FeO-rich chondrules contain albite-rich plagioclase (An<sub>15–55</sub>; Kunihiro et al., 2004; Kurahashi et al., 2008). According to Co partitioning in Fe, Ni metals, the metamorphic temperature of Y-81020 is estimated to be 400–500 °C (e.g., Kimura et al., 2008). At these temperatures, albite-rich plagioclase grains might lose some of their <sup>26</sup>Mg excess, especially considering their small grain sizes (≤10 μm), so that the formation ages of these chondrules would be older than those estimated from the isochron diagram. In contrast, younger chondrules (>3 Ma after CAI formation) in CR chondrites are mostly Mg-rich chondrules with plagioclase near the anorthite end member (e.g., Hutcheon et al., 2009; Tenner et al., 2013). Therefore, the Al–Mg ages of chondrules in CR chondrites might not be affected by parent body processes in the CR chondrite parent body, and chondrule formation ages likely extended to more than 3 Ma after CAIs in CR chondrite forming regions.

### Acknowledgements

The authors thank Mike Krawczynski for assistance with error analysis and discussions on other aspects of the data, Jim Kern for assistance with profilometer analysis, and two anonymous reviewers for helpful comments. This work was supported by the NASA Cosmochemistry program (NNX09AB-93G). WiscSIMS is partly supported by NSF (EAR03-19230, EAR07-44079, EAR10-53466).

### References

- Amelin, Y., Krot, A.N., Hutcheon, I.D., Ulyanov, A.A., 2002. Lead isotopic ages of chondrules and calcium–aluminum-rich inclusions. *Science* 297, 1678–1683.
- Amelin, Y., Kaltenbach, A., Lizuka, T., Stirling, C.H., Ireland, T.R., Pataev, M., Jacobsen, S.B., 2010. U–Pb chronology of the Solar System's oldest solids with variable <sup>238</sup>U/<sup>235</sup>U. *Earth Planet. Sci. Lett.* 300, 343–350.
- Balluffi, R.W., 1960. On the determination of diffusion coefficients in chemical diffusion. *Acta Metall.* 8, 871–873.
- Behrens, H., Johannes, W., Schmalzried, H., 1990. On the mechanisms of cation diffusion processes in ternary feldspars. *Phys. Chem. Miner.* 17, 62–78.
- Bevington, P.R., Robinson, D.K., 2002. *Data Reduction and Error Analysis for the Physical Sciences*, 3rd ed. McGraw–Hill.
- Brennecka, G.A., Weyer, S., Wadhwa, M., Janney, P.E., Zipfel, J., Anbar, A.D., 2010. <sup>238</sup>U/<sup>235</sup>U variations in meteorites: Extant <sup>247</sup>Cm and implications for Pb–Pb dating. *Science* 327, 449–451.
- Chakraborty, S., Farver, J.R., Yund, R.A., Rubie, D.C., 1994. Mg tracer diffusion in synthetic forsterite and San Carlos olivine as a function of P, T and *f*<sub>O<sub>2</sub></sub>. *Phys. Chem. Miner.* 21, 499–500.
- Cherniak, D.J., 1995. Diffusion of lead in plagioclase and K-feldspar: an investigation using Rutherford backscattering and resonant nuclear reaction analysis. *Contrib. Mineral. Petrol.* 120, 358–371.
- Cherniak, D.J., 2002. Ba diffusion in feldspar. *Geochim. Cosmochim. Acta* 66, 1641–1650.
- Cherniak, D.J., 2003. REE diffusion in feldspar. *Chem. Geol.* 193, 273–287.
- Cherniak, D.J., 2010. Cation diffusion in feldspars. *Rev. Mineral. Geochem.* 72, 691–733.
- Cherniak, D.J., Lanford, W.A., Ryerson, F.J., 1991. Lead diffusion in apatite and zircon using ion implantation and Rutherford Backscattering techniques. *Geochim. Cosmochim. Acta* 55, 1663–1673.
- Cherniak, D.J., Watson, E.B., 1992. A study of strontium diffusion in K-feldspar, Na–K feldspar and anorthite using ion implantation and Rutherford backscattering spectroscopy. *Earth Planet. Sci. Lett.* 113, 411–425.
- Cherniak, D.J., Watson, E.B., 1994. A study of strontium diffusion in plagioclase using Rutherford Backscattering spectroscopy. *Geochim. Cosmochim. Acta* 58, 5179–5190.
- Connelly, J.N., Bizzarro, M., Krot, A.N., Nordlund, A., Wielandt, D., Ivanova, M.A., 2012. The absolute chronology and thermal processing of solids in the solar protoplanetary disk. *Science* 338, 651–655.
- Costa, F., Chakraborty, S., Dohmen, R., 2003. Diffusion coupling between trace and major elements and a model for calculation of magma residence times using plagioclase. *Geochim. Cosmochim. Acta* 67, 2189–2200.
- Costa, F., Dohmen, R., Chakraborty, S., 2008. Timescales of magmatic processes from modeling the zoning patterns of crystals. *Rev. Mineral. Geochem.* 69, 545–594.
- Crank, J., 1975. *The Mathematics of Diffusion*, 2nd ed. Clarendon Press, Oxford.
- Desch, S.J., Connolly, H.C. Jr., 2002. A model of the thermal processing of particles in solar nebula shocks: Application to the cooling rates of chondrules. *Meteorit. Planet. Sci.* 37, 183–207.
- Dodson, M.H., 1973. Closure temperature in cooling geochronological and petrological systems. *Contrib. Mineral. Petrol.* 40, 259–264.
- Druitt, T.H., Costa, F., Deloule, E., Dungan, M., Scaillet, B., 2012. Decadal to monthly timescales of magma transfer and reservoir growth at a caldera volcano. *Nature* 482, 77–82.
- Faak, K., Chakraborty, S., Coogan, L.A., 2013. Mg in plagioclase: Experimental calibration of a new geothermometer and diffusion coefficients. *Geochim. Cosmochim. Acta* 123, 195–217.
- Ganguly, J., Tirone, M., 1999. Relationship between cooling rate and cooling age of a mineral: Theory and applications to meteorites. *Meteorit. Planet. Sci.* 36, 167–175.
- Ganguly, J., Tirone, M., Chakraborty, S., Domanik, K., 2013. H-chondrite parent asteroid: A multistage cooling, fragmentation and re-accretion history constrained by thermometric studies, diffusion kinetic modeling and geochronological data. *Geochim. Cosmochim. Acta* 105, 206–220.
- Giletti, B.J., Casserly, J.E.D., 1994. Sr diffusion kinetics in plagioclase feldspars. *Geochim. Cosmochim. Acta* 58, 3785–3793.
- Goodrich, C.A., Hutcheon, I.D., Kita, N.T., Huss, G.R., Cohen, B.A., Keil, K., 2010. <sup>53</sup>Mn–<sup>53</sup>Cr and <sup>26</sup>Al–<sup>26</sup>Mg ages of a feldspathic lithology in polymict ureilites. *Earth Planet. Sci. Lett.* 295, 531–540.
- Göpel, C., Manhès, G., Allègre, C.J., 1994. U–Pb systematics of phosphates from equilibrated chondrites. *Earth Planet. Sci. Lett.* 121, 153–171.
- Grove, T.L., Baker, M.B., Kinzler, R.J., 1984. Coupled CaAl–NaSi diffusion in plagioclase feldspar: experiments and applications to cooling rate speedometry. *Geochim. Cosmochim. Acta* 48, 2113–2121.
- Huss, G.R., MacPherson, G.J., Wasserburg, G.J., Russell, S.S., Srinivasan, G., 2001. <sup>26</sup>Al in CAIs and chondrules from unequilibrated ordinary chondrites. *Meteorit. Planet. Sci.* 36, 975–997.
- Hutcheon, I.D., Marhas, K.K., Krot, A.N., Goswami, J.N., Jones, R.H., 2009. <sup>26</sup>Al in plagioclase-rich chondrules in carbonaceous chondrites: Evidence for an extended duration of chondrule formation. *Geochim. Cosmochim. Acta* 73, 5080–5099.
- Ito, M., Ganguly, J., 2006. Diffusion kinetics of Cr in olivine and <sup>53</sup>Mn–<sup>53</sup>Cr thermochronology of early solar system objects. *Geochim. Cosmochim. Acta* 70, 799–809.
- Kimura, M., Grossman, J.N., Weisberg, M.K., 2008. Fe–Ni metal in primitive chondrites: indicators of classification and metamorphic conditions for ordinary and CO chondrites. *Meteorit. Planet. Sci.* 43, 1161–1177.
- Kita, N.T., Ushikubo, T., 2012. Evolution of protoplanetary disk inferred from <sup>26</sup>Al chronometry of individual chondrules. *Meteorit. Planet. Sci.* 47, 1108–1119.
- Kita, N.T., Ushikubo, T., Knight, K.B., Mendybaev, R.A., Davis, A.M., Richter, F.M., Fournelle, J.H., 2012. Internal <sup>26</sup>Al–<sup>26</sup>Mg isotope systematics of a type B CAI: Remelting of refractory precursor solids. *Geochim. Cosmochim. Acta* 86, 37–51.
- Kita, N.T., Yin, Q.-Y., MacPherson, G.J., Ushikubo, T., Jacobsen, B., Nagashima, K., Kurahashi, E., Krot, A.N., Jacobsen, S.B., 2013. <sup>26</sup>Al–<sup>26</sup>Mg isotope systematics of the first solids in the early Solar System. *Meteorit. Planet. Sci.* 48, 1383–1400.
- Kunihiro, T., Rubin, A.E., McKeegan, K.D., Wasson, J.T., 2004. Initial <sup>26</sup>Al/<sup>27</sup>Al in carbonaceous-chondrite chondrules: Too little <sup>26</sup>Al to melt asteroids. *Geochim. Cosmochim. Acta* 68, 2947–2957.
- Kurahashi, E., Kita, N.T., Nagahara, H., Morishita, Y., 2008. <sup>26</sup>Al–<sup>26</sup>Mg systematics of chondrules in a primitive CO chondrite. *Geochim. Cosmochim. Acta* 72, 3865–3882.
- LaTourrette, T., Wasserburg, G.J., 1998. Mg diffusion in anorthite: implications for the formation of early solar system planetesimals. *Earth Planet. Sci. Lett.* 158, 91–108.
- Lee, T., Papanastassiou, D.A., Wasserburg, G.J., 1977. Aluminum-26 in the early solar system – fossil or fuel. *Astrophys. J.* 211, L107–L110.
- Longhi, J., Hays, J.F., 1979. Phase equilibria and solid solution along the join CaAl<sub>2</sub>Si<sub>2</sub>O<sub>8</sub>–SiO<sub>2</sub>. *Am. J. Sci.* 279, 876–890.
- MacPherson, G.J., Davis, A.M., Zinner, E.K., 1995. The distribution of aluminum-26 in the early solar system: A reappraisal. *Meteoritics* 30, 365–386.
- MacPherson, G.J., Kita, N.T., Ushikubo, T., Bullock, E.S., Davis, A.M., 2012. Well-resolved variations in the formation ages for Ca–Al-rich inclusions in the early Solar System. *Earth Planet. Sci. Lett.* 331–332, 43–54.
- Nagashima, K., Krot, A.N., Chaussidon, M., 2007. Aluminum–magnesium isotope systematics of chondrules from CR chondrites. *Meteorit. Planet. Sci. Suppl.* 42, 5291.
- Nagashima, K., Krot, A.N., Huss, G., 2008. <sup>26</sup>Al in chondrules from CR carbonaceous chondrites. In: 39th Lunar Planetary Science Conference, abstract #2224.
- Russell, S.S., Srinivasan, G., Huss, G.R., Wasserburg, G.J., MacPherson, G.J., 1996. Evidence for widespread <sup>26</sup>Al in the solar nebula and constraints for nebula timescales. *Science* 273, 757–762.
- Shewmon, P., 1989. *Diffusion in Solids*, 2nd ed. Minerals, Metals & Materials Society, Warrendale, Pennsylvania, USA.
- Srinivasan, G., Goswami, J.N., Bhandari, N., 1999. <sup>26</sup>Al in eucrite Piplia Kalan: Plausible heat source and formation chronology. *Science* 284, 1348–1350.
- Tenner, T.J., Ushikubo, T., Nakashima, D., Kita, N.T., Weisberg, M.K., 2013. <sup>26</sup>Al in chondrules from the CR3.0 chondrite Queen Alexandra Range 99177: A link with O isotopes. In: 44th Lunar Planetary Science Conference, abstract #2010.
- Valley, J.W., Kita, N., 2009. In situ oxygen isotope geochemistry by ion microprobe. *Mineral. Assoc. Can. Short Course* 41, 19–63. Toronto.

- Van Orman, J.A., Grove, T.L., Shimizu, N., 2001. Rare earth element diffusion in diopside: influence of temperature, pressure, and ionic radius, and an elastic model for diffusion in silicates. *Contrib. Mineral. Petrol.* 141, 687–703.
- Van Orman, J.A., Saal, A.E., Bourdon, B., Hauri, E.H., 2006. Diffusive fractionation of U-series radionuclides during mantle melting and shallow level melt-cumulate interaction. *Geochim. Cosmochim. Acta* 70, 4797–4812.
- Watson, E.B., 1982. Basalt contamination by continental crust: some experiments and models. *Contrib. Mineral. Petrol.* 80, 73–87.
- Zhang, Y., Walker, D., Leshner, C.E., 1989. Diffusive crystal dissolution. *Contrib. Mineral. Petrol.* 102, 492–513.
- Zinner, E., Göpel, C., 2002. Aluminum-26 in H4 chondrites: Implications for its production and its usefulness as a fine-scale chronometer for early solar system events. *Meteorit. Planet. Sci.* 37, 1001–1013.